Impact of spatial variations of land surface parameters on regional evaporation: a case study with remote sensing data

Hussein O. Farah[1] and Wim G. M. Bastiaanssen[2]*

[1] *Department of Civil and Structural Engineering, Moi University, P.O. Box 3900, Eldoret, Kenya*
[2] *Division of Water Resources and Environmental Studies, International Institute for Aerospace Survey and Earth Sciences (ITC),*
P.O. Box 6, 7500 AA, Enschede, The Netherlands

Abstract:

Most precipitation in watersheds is consumed by evaporation, thus techniques to appraise regional evaporation are important to assess the availability of water resources. Many algorithms to estimate evaporation from remotely sensed spectral data have been developed in the recent past. In addition to differences in the physical parameterization of surface fluxes, these algorithms have different solutions for describing spatial variations of the parameters in the soil–vegetation–atmosphere–transfer (SVAT) continuum. In this study, the necessity to spatially distinguish SVAT parameters for computing surface heat fluxes is analysed for the Naivasha watershed in the Kenyan Rift Valley. Landsat Thematic Mapper (TM) spectral data have been used to first delineate the watershed into 15 hydrological units using surface temperature, normalized difference vegetation index and surface albedo as attributes. Thereafter, semi-empirical relationships between these TM-based parameters and other SVAT parameters have been applied to compute the spatial variation of SVAT parameters and the associated evaporation from the different hydrological units. The impact of using watershed-constant or watershed-distributed SVAT parameters on the fluxes is analysed. The determination of watershed averaged evaporation with area-aggregated SVAT parameters is feasible without significant loss of accuracy. Distributed evaporation in heterogeneous watersheds, however, can be investigated only with remote sensing flux algorithms that can account for spatially variable air temperature, surface roughness, surface albedo and the stability correction of the temperature profile due to buoyancy. Erroneous results can be expected if area-aggregated SVAT parameters are used to calculate local evaporation. As most of the recently developed remote sensing flux algorithms are based on areal constant SVAT parameters, direct applications in watersheds are still limited. Copyright © 2001 John Wiley & Sons, Ltd.

KEY WORDS   evapotranspiration; remote sensing; spatial variations of SVAT parameters; Lake Naivasha basin

INTRODUCTION

Sensible (H) and latent heat fluxes (LE) vary spatially because of the heterogeneity of soil physical properties, terrain slope, land cover, and water influx through precipitation, irrigation and groundwater. The parameters of the soil–vegetation–atmosphere–transfer continuum exhibit a distinct spatial variation in watersheds. The spatial scale may vary from less than a metre to the size of the watersheds. Time variations in term of hours may be significant. Ground measurements of land surface fluxes are representative of a relatively small area. Land surface fluxes at the regional scale therefore are difficult to deduce from a limited number of *in situ* field stations equipped with advanced measurement devices. Satellite remote sensing methods have been used in the last 20 years to overcome these discrepancies in scale. The fluxes from one pixel up to the watershed scale can be estimated by means of remotely sensed data. Most of these remote sensing techniques are based on spectral measurements in the visible, near-infrared and thermal infrared portions of the electromagnetic

---

*Correspondence to: W. G. M. Bastiaanssen, ITC, P.O. Box 6, 7500 AA, Enschede, The Netherlands. E-mail: bastiaanssen@itc.nl

spectrum. Moran and Jackson (1991) and Kustas and Norman (1996) have made a review of some of these techniques.

Remotely sensed multispectral measurements have been used to estimate parameters of soil–vegetation–atmosphere–transfer models (i.e. SVAT parameters). Surface temperature, T_0, is the most common SVAT parameter used to interpret spatial variation in evaporation (e.g. Jackson *et al*., 1977), however, attempts have been made with many other SVAT parameters to explain variability in evaporation, soil moisture (Chen *et al*., 1997), fractional vegetation cover v_c (Choudhury *et al*., 1994), leaf area index (Baret and Guyot, 1991), surface albedo r_0 (Jackson, 1984), surface thermal infrared emissivity ε_0, (Valor and Caselles, 1996), air temperature T_a (Prihodko and Goward, 1997), crop height (Moran *et al*., 1995) and surface roughness length for momentum transport z_{0m} (Moran and Jackson, 1991).

The sensible heat and latent heat fluxes can be parameterized as a simple linear function of T_0, or the difference between surface and air temperature. For instance, Seguin and Itier (1983) explained variation in evaporation to variation in surface temperature. This concept may correctly describe the fluxes emerging from homogeneous landscapes, e.g. agricultural systems with uniform crop stands and other biophysical properties. For heterogeneous watersheds with distinct variation in SVAT parameters and fluxes, however, the assumption of linearity between T_0 and fluxes does not hold, and involvement of other SVAT parameters becomes essential. The relationship between fluxes and T_0 portrayed in Figure 1A for simultaneously measured T_0 and *LE* fluxes at 12 stations in the catchment of the Guadiana River (central Spain) indicates that the variance of fluxes cannot be explained by variations in T_0 alone. The scatter can be explained only by other scale variant SVAT parameters. Figure 1B shows the achievements of an integrated SVAT–boundary-layer model study conducted by Blyth (1994), which reveals, on the basis of general physics, that *LE* variations are not ascribed to variations in T_0 only.

Furthermore, surface energy balance models using remote sensing are based mostly on one dimensional representation of the momentum and heat exchanges between the land and atmosphere (see Figure 2). The selection of vertical length scale Z_{sur} has impacts for the quantification and spatial variability of, for example, T_a and aerodynamic resistance, r_{ah} (and hence roughness length for heat transport z_{oh}, frictional velocity u_* and stability correction factor Ψ_h). If Z_{sur} is taken to be at some height, usually referred to as blending height, in the planetary boundary layer where fluxes are independent of surface features, then T_a and r_{ah} become spatially constant. As the spatial variation of T_a at the blending height for heat is eliminated by advection, however, the sensible heat flux between the land surface and the blending height is not strictly
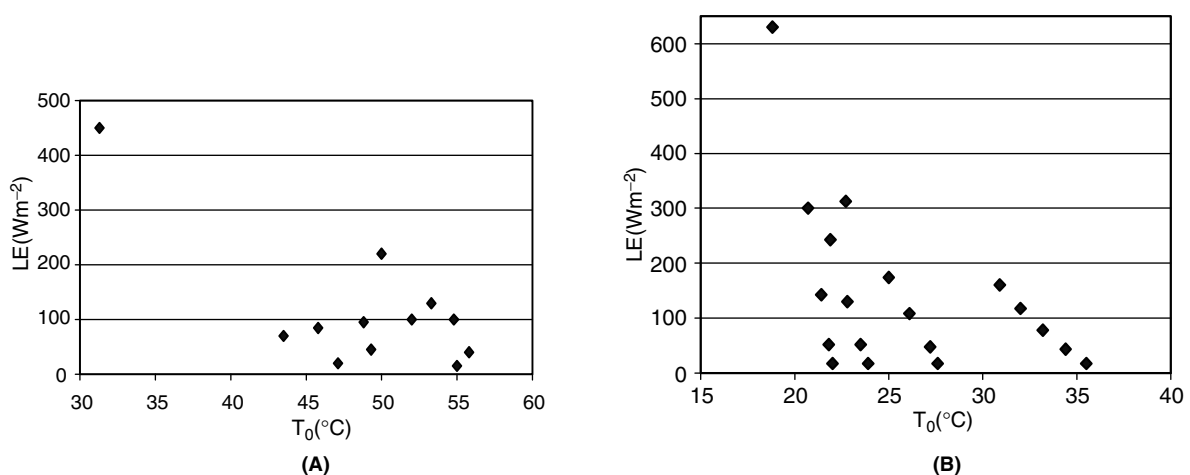

Figure 1. Latent heat flux as a function of surface temperature. (A) Field measurements in Castilla la Mancha (Pelgrum and Bastiaanssen, 1997). (B) Model simulation in a patchy landscape with intermittent wet and dry surfaces (Blyth, 1994)
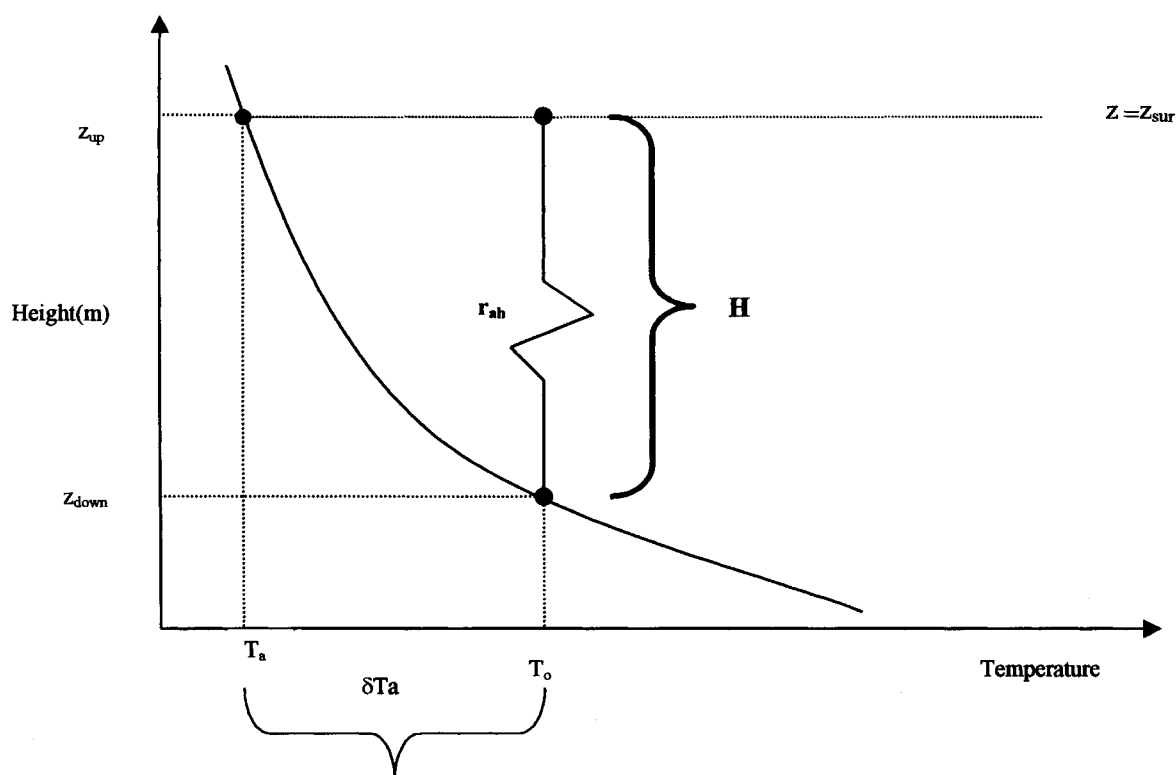
Figure 2. Theoretical profiles of air temperature (T_a) in relation to integration limits (z_{down} and z_{up}) affecting the aerodynamic resistance to heat transport (r_{ah}) and the radiometric surface temperature (T_0)

one dimensional. If the purpose of study is to determine near-surface spatial variations of fluxes, Z_{sur} has to be kept small and advection may be ignored (Bastiaanssen *et al.*, 1996). At near- surface level (2 to 10 m) there are differences in T_a and r_{ah} in the horizontal domain. These horizontal gradients are caused by the underlaying local hydrometeorological processes and have consequences for the way the spatial variations of SVAT parameters are schematized in the remote sensing algorithms, if correct fluxes have to be obtained. Table I shows how different categories of remote sensing algorithms treat spatial variations of T_a and r_{ah} (z_{oh}, u_* and Ψ_h). It is evident that most algorithms take T_a either at $Z_{sur} \approx 2$ m or at larger height $Z_{sur} \approx 100$ m that is spatially constant. Table I also shows that u_* (i.e. momentum flux) is considered spatially constant by all algorithms except class 5. It therefore is prudent to investigate the influence of spatial variability of SVAT parameters on surface fluxes for heterogeneous landscapes so as to identify the parameters that should be treated minimally as spatially variable and which can be taken as spatially constant.

The modelling of spatial heterogeneity usually is achieved by delineating the surface into units of homogeneous hydrological characteristics and deriving SVAT parameters for each unit from which fluxes can be determined. The first objective of this study is to demonstrate how a complex watershed can be delineated into hydrological units or partial areas with the help of satellite remote sensing. Watersheds with little data availability are the norm in both developing and developed countries and remotely sensed information is very useful to describe heterogeneous landscapes and related land surface processes. The second objective is the assessment of SVAT parameters and the accompanying surface fluxes of each hydrological unit discerned from the remote sensing measurements. The third objective is to study the consequences of using spatially constant SVAT parameters or watershed-distributed SVAT parameters on evaporation.

Table I. Application studies using conceptually different solutions for T_a and r_{ah} (c = spatially constant, v = spatially variable, n = not considered) (adapted from Bastiaanssen *et al.*, 1996)

Classes of H-schematization	T_a $Z_{sur} \approx 2$ m	T_a $Z_{sur} \approx 100$ m	z_{oh}	u^*	Ψ_h	References
Class 1	c	n	c	c	n	Jackson *et al.*, 1977; Seguin and Itier, 1983
Class 2	c	n	v	c	c	Kustas *et al.*, 1994; Kalma and Jupp, 1990
Class 3	n	c	c	c	c	Rosema, 1990; Brutsaert *et al.*, 1993
Class 4	n	c	v	c	c	Menenti and Choudhury, 1994; Diak and Whipple, 1993
Class 5	V	c	v	v	v	Carlson and Buffum, 1989; Bastiaanssen *et al.*, 1998a

ESTIMATION OF BASIC SURFACE RADIOMETRIC PARAMETERS

Landsat Thematic Mapper (TM) measures the spectral radiances in the visible, near, middle and thermal infrared spectrum at the top of the atmosphere. A TM scene of 21 January 1995, covering the Lake Naivasha watershed in Kenya, has been used in the current analysis. The TM has three bands in the visible, three bands in the near- and middle infrared and one band in the thermal infrared spectral region. The digital values of each pixel are converted first to spectral radiance at the top of the atmosphere using a radiometric calibration procedure (Markham and Barker, 1987). The broad band planetary albedo at the top of the atmosphere (r_p) is calculated with a weighing scheme of the six visible and near-infrared bands (TM 1, 2, 3, 4, 5 and 7) and spectral radiation incident at the top of the atmosphere. The broad band planetary albedo (r_p) is related to the broad band surface albedo (r_0) through a simple linear relationship (e.g. Zhong and Li, 1988)

$$r_0 = \frac{r_p - r_a}{\tau''_{sw}} \qquad (-) \tag{1}$$

where r_a (−) is the lowest planetary albedo of all pixels (i.e. r_p^{min}) being usually an area with a negligible small surface albedo and τ''_{sw} (−) is the two-way transmittance for broad band solar radiation (0·3 to 3·0 μm). This simple atmospheric correction for broad band short-wave radiation takes into account the atmospheric transmittance and the path radiance (see also Koepke *et al.*, 1985). Choudhury (1991) and Pinty and Ramond (1987) report a relative error of 10% using simple corrections such as equation (1). The correction is valid for an albedo range from 0·05 to 0·43, as reported by Menenti *et al.*, (1989). In this case study, the two-way transmittance was estimated by taking the surface albedo of Lake Naivasha to be $r_0 = 0·06$. This generally is the accepted value for albedo for shallow water bodies (de Bruin and Keijman, 1979) and also was confirmed by fields measurements in Lake Naivasha (see Figure 6B). This yields a calibration of $\tau''_{sw} = 0·35$ at $r_a = 0·01$.

The thermal channel, TM_6, measures the spectrally emitted radiance between 10·6 and 12·4 μm at the top of the atmosphere, L_6^{TOA}, which can be interpreted from the raw digital numbers (DN_6) in band 6 (Markham and Barker, 1987)

$$L_6^{TOA} = [0·1238 + (1·560 - 0·1238) \times DN_6/255] \times \pi \times B \times 10 \qquad (\text{W m}^{-2}) \tag{2}$$

where B (μm) is the band width of the thermal channel (12·4−10·6 = 1·8 μm) and DN_6 is the digital number of TM band 6. The spectral radiances at the top of the atmosphere measured by the satellite are related to the spectrally emitted radiances at the land surface L_6^{surf} (e.g. Schmugge *et al.*, 1998)

$$L_6^{TOA} = L_6^{surf}\tau_6 + L_6^{atm} \qquad (\text{W m}^{-2}) \tag{3}$$

where L_6^{atm} is the long-wave radiation emitted from the atmosphere upwards (i.e. thermal path radiance) and τ_6 (−) is the atmospheric transmittance in the region $\lambda = 10·6$ to 12·4 μm. Usually, L_6^{atm} and τ_6 are
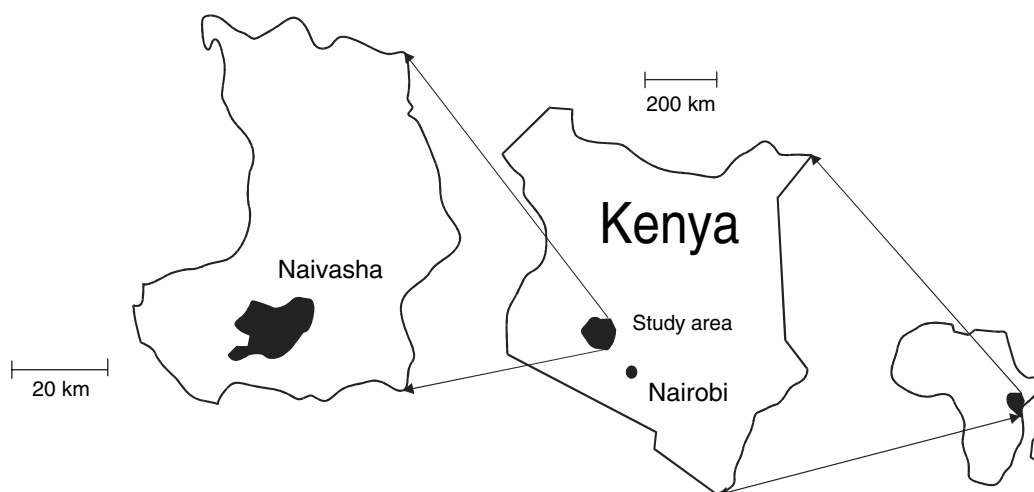
Figure 3. Location of the Lake Naivasha watershed, Kenya

determined by atmospheric radiation transfer models (e.g. Tanre *et al*., 1990) or from a limited number of T_0 field measurements acquired at the same moment of the satellite overpass. As these instantaneous field measurements were not available for the Lake Naivasha area, a trial and error procedure has been applied (Ashfaque, 1999). The spectral radiances at surface level were, after atmospheric correction, converted into radiometric surface temperature through the inversion of Planck's law

$$T_0 = \frac{14\,388}{11 \cdot 5 \ln[(\frac{\varepsilon_0 \times B \times 3 \cdot 7427 \times 10^8}{L_6^{\text{surf}}}) + 1]} \quad \text{(K)} \tag{4}$$

where ε_0 (−) is the thermal infrared surface emissivity in the spectral range of TM band 6 and T_0 (K) is the radiometric surface temperature corrected for grey body effects. Results indicate that T_0 ranges at pixel scale between $22 \cdot 2\,°C$ to $44 \cdot 0\,°C$. For Lake Naivasha, an average value of $24 \cdot 8\,°C$ was obtained. The daytime water temperature of Lake Naivasha in the month of January is known to vary between 22 and $26\,°C$ (Donia, 1998). Hence, the T_0 values are reasonable.

The thermal infrared surface emissivity is estimated on the basis of the normalized difference vegetation index (NDVI) (van de Griend and Owe, 1993)

$$\varepsilon_0 = 1 \cdot 009 + 0 \cdot 047 \ln(\text{NDVI}) \quad (-) \tag{5}$$

A theoretical justification of the relationship between ε_0 and NDVI is given by Valor and Caselles, (1996). They report an error of $0 \cdot 6\%$ in estimating ε_0 from Equation (5) for mid-latitudes and tropical regions. The relationship between ε_0 and NDVI is valid for the NDVI values in the range $0 \cdot 16$ to $0 \cdot 74$. This equation is hence not valid for water bodies with a negative NDVI. Therefore, the water bodies were masked and forced with $\varepsilon_0 = 1 \cdot 0$. The NDVI can give information on vegetation density, colour of the surface and cultivation practices. This is due to the property of chlorophyll, which strongly absorbs radiation in the red parts of the electromagnetic spectrum and reflects it in the near-infrared part (Tucker, 1979). It is determined as follows

$$\text{NDVI} = \frac{r_p(4) - r_p(3)}{r_p(4) + r_p(3)} \quad (-) \tag{6}$$

where $r_p(4)$ and $r_p(3)$ are the spectral planetary reflectances for TM bands 4 and 3 respectively.

HYDROLOGICAL DELINEATION OF THE KENYAN CENTRAL RIFT VALLEY

The Lake Naivasha basin located in central Kenya was selected for this study. The Lake Navaisha basin is part of the East African Rift Valley and covers an area of about 3000 km^2 (Figure 3). The valley has a relatively flat bottom of 45 to 70 km wide and runs in a north–south direction. The altitude varies from about 1900 to 2800 m, and these differences induce a variation in the areal patterns of precipitation. The mean annual rainfall varies from 600 to 1000 mm/year. The area therefore has a diverse landscape, ranging from forests in the mountains to dry range lands in the valley. Rain-fed crops, swamps and barren land composed of rock outcrops and unvegetated lava flows also are present. Extensive irrigation is practiced on flowers and vegetables in the vicinity of Lake Naivasha, and pastures also are irrigated for cattle grazing. There has been an increasingly large demand for water in the basin during the last 30 years owing to the high population increase of up to 70% (Ase *et al*., 1986). The high population increase is attributed to immigration of people from other parts of the country to settle in what was formerly called the white highlands.

Segmentation of landscapes traditionally is done by using land-use/land-cover maps, topographic maps, soil maps, etc. The purpose of partial area hydrology is to handle the large amount of hydrological variability in watersheds by a few units. Hydrological units simplify the characterization of a watershed into a small finite number of subareas having less internal variability, but describing together the overall hydrological response to rainfall and irrigation. Through mass conservation, evaporation is related indirectly to rainfall, runoff, irrigation and groundwater movement. Past studies have shown that T_0 is an indicator of evaporation (e.g. Jackson *et al*., 1977) and that a scatter plot of T_0 versus NDVI reflects spatial variations in fractional vegetation cover (v_c), soil water content (θ) and surface resistance to evaporation r_s (e.g. Nemani and Running, 1989). The $T_0(r_0)$ relationship also has been proven to be valuable for determining dry and wet land surface types (Menenti *et al*., 1989). Figure 4 shows the relationships between T_0, NDVI and r_0, reflecting different land wetness conditions and vegetation cover. The NDVI, r_0 and T_0 values of all the pixels in the image are plotted in a three-dimensional space given by the *XYZ* axis. First a regularly spaced array of Z (T_0) values from the irregularly spaced *XYZ* data is produced by interpolation methods. Next a surface is fitted to the regularly spaced T_0 values by a least-squares-fit approach. Qualitative interpretation of the hydrological and vegetation status of subareas can be made: low T_0, low NDVI and low r_0 indicates bare wet soils, whereas high T_0, low NDVI and high r_0 presents the warm, dry, bare soil pockets. Low T_0, high NDVI and low r_0 indicates healthy vegetation in good condition having unstressed transpiration, whereas high T_0, high NDVI and high r_0 point to vegetation under water stress. As T_0, NDVI and r_0 can, according to Equations (1) to (6), be retrieved from Landsat TM, and as they reveal hydrological conditions, the watershed can be delineated from T_0, r_0 and NDVI.

A cluster analysis based on T_0, NDVI and r_0 therefore was performed, which divided the study area into 15 clusters (Figure 5). There are about 50 000 pixels in the 19 km by 25 km study area. Clustering was carried out in order to reduce this large number of pixels and group them into 15 units. This number of units was chosen from prior knowledge of the area in which 15 different land-use and land-cover types were identified from ground survey and aerial photography (Hamududu, 1998). The clustering algorithm groups the pixels based on the statistical properties of the pixels. A generalized form of the Heckbert quantization algorithm (Heckbert, 1994) is used. First a multidimensional histogram of the input values of T_0, r_0 and NDVI values of the pixels is created. This multidimensional space of 'cloud of points' is divided into the 15 clusters. The algorithm starts with the whole space as one cluster and finds the axis with the largest variations in pixel values. The cluster is divided into two along the calculated axis. Similarly the new clusters are further divided until the desired 15 clusters are achieved.

The T_0, NDVI and r_0 values for the clusters discerned are presented in Table II. The 15 units represent areas with different wetness conditions, not variations in land use/land cover per se. The wettest and driest units are units 2 and 14 respectively. Unit 2 represents open water ($T_0 = 24 \cdot 8\,^\circ$C; NDVI $= -0 \cdot 3$; $r_0 = 0 \cdot 06$), whereas unit 14 consists of sparse vegetation and bare land, having a high radiometric surface temperature, implying that evaporation is minimum ($T_0 = 36 \cdot 7\,^\circ$C; NDVI $= 0 \cdot 37$; $r_0 = 0 \cdot 25$). These area correspond to rock outcrops

Figure 4. Relationship between surface temperature, NDVI and surface albedo
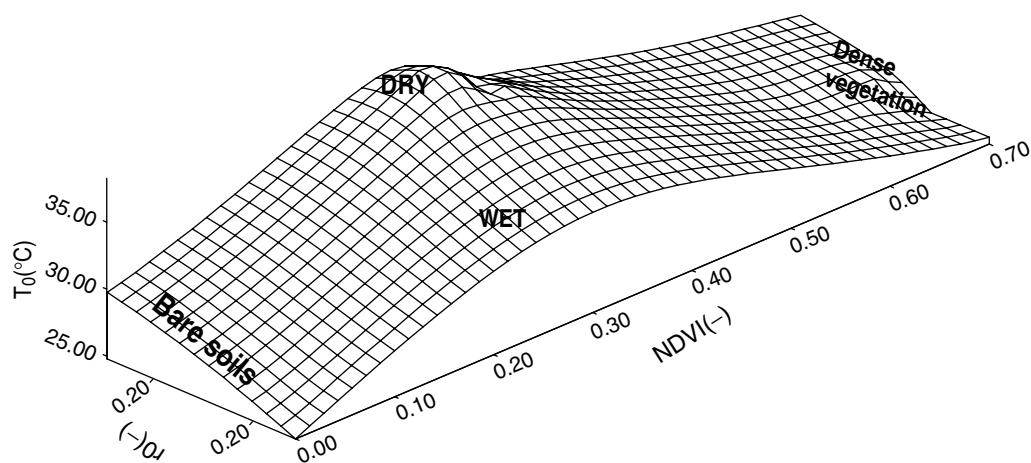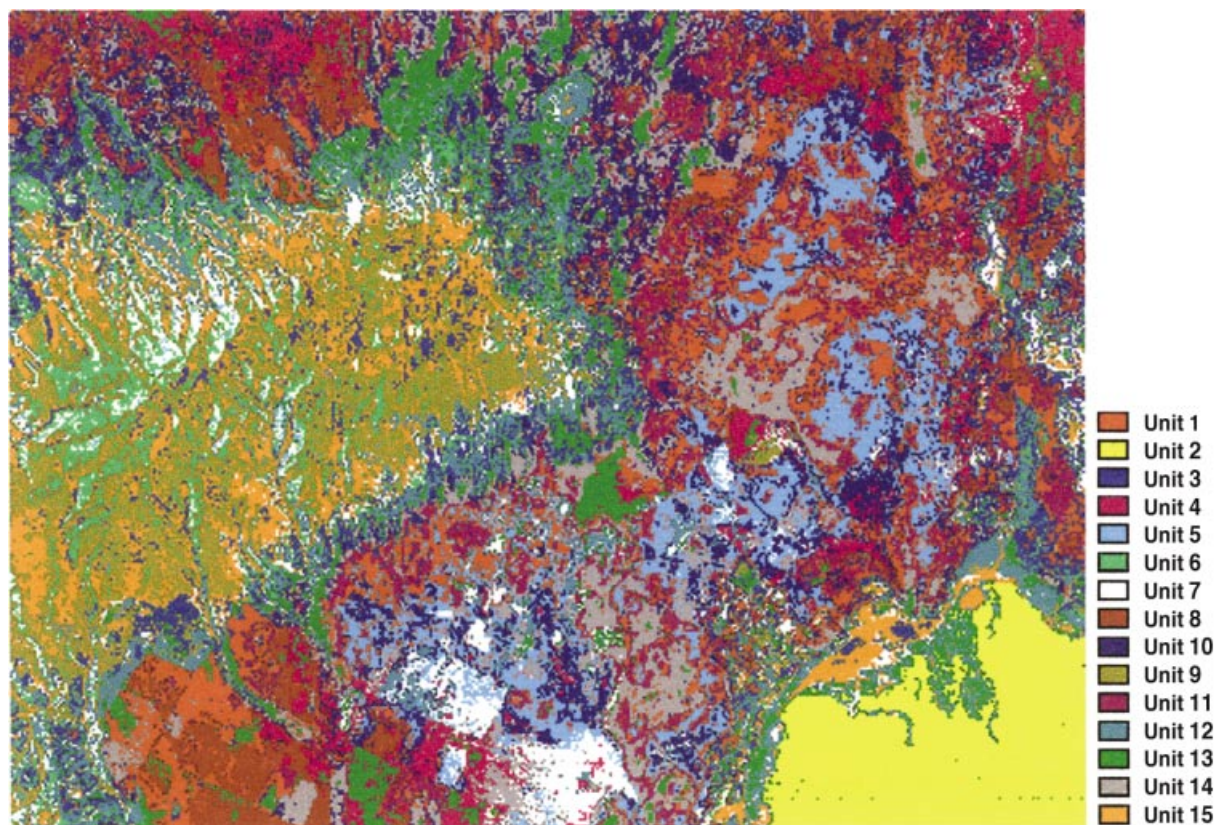

Figure 5. Hydrological delineation of Lake Naivasha watershed based on surface temperature, NDVI and surface albedo using a cluster analysis

and bare lava flows identified on topographic maps of the area. Between these two hydrological extremes are the forested Eburu hills in the western part of the watershed and also swamp and river embankment vegetation

Table II. Values of radiometric surface temperature (T_0), nor-
malized difference vegetation index(NDVI) and surface albedo
(r_0) for the 15 hydrological units

Hydrological unit	Area %	T_0 (°C)	NDVI (−)	r_0 (−)
1	7·81	33·9	0·40	0·19
2	22·20	24·8	−0·30	0·06
3	1·40	26·6	0·66	0·12
4	1·05	38·1	0·30	0·20
5	12·85	38·4	0·29	0·22
6	2·36	28·0	0·59	0·14
7	9·75	37·3	0·32	0·21
8	3·84	35·8	0·35	0·21
9	1·34	25·3	0·70	0·12
10	6·20	35·5	0·33	0·20
11	11·45	34·1	0·37	0·25
12	4·06	36·7	0·30	0·18
13	6·17	36·4	0·34	0·19
14	8·84	36·7	0·37	0·25
15	0·68	28·0	0·67	0·15
Total	100·0			

(units 6, 9 and 15). Hydrological unit 9 must transpire more than units 6 and 15 owing to the lower T_0 and higher NDVI value. This can be concluded even without having access to ground data. The irrigated areas are found in the direct vicinity of Lake Navaisha (unit 3) and they may comprise several horticultural activities. The drier areas with low vegetation cover are represented by range lands with high T_0, low NDVI and high r_0. These units (4, 5 and 7) are found in the central parts of the study area, being part of the natural ecosystems.

ESTIMATION OF SVAT PARAMETERS AND SURFACE FLUXES FOR EACH HYDROLOGICAL UNIT

Net available energy (R_n, G_0)

Under non-advective conditions and neglecting heat storage in canopies, surface fluxes have to satisfy the preservation of energy

$$R_n + G_0 + H + LE = 0 \qquad (\text{W m}^{-2}) \tag{7}$$

where R_n is the net radiation, G_0 the soil heat flux, H the sensible heat flux and LE the latent heat flux required for evaporation. The energy balance equation can be decomposed further into its constituent parameters. Net radiation is calculated as the sum of incoming and outgoing short-wave and long-wave radiation components

$$R_n = (1 - r_0)K^{\downarrow} + \varepsilon'\sigma T_a^4 - \varepsilon_0\sigma T_0^4 - (1 - \varepsilon_0)\varepsilon'\sigma T_a^4 \qquad (\text{W m}^{-2}) \tag{8}$$

where $K^{\downarrow}$ (W m^{-2}) is the incoming short wave solar radiation, $\varepsilon'\sigma T_a^4$ (W m^{-2}) is the incoming long-wave radiation emitted by the atmosphere, with ε' (−) being the apparent emissivity of the atmosphere, σ (W m^{-2} K^{-4}) is the Stefan–Boltzmann constant, T_a (K) is the screen height air temperature, and $\varepsilon_0\sigma T_0^4$ (W m^{-2}) is the outgoing long-wave radiation emitted by the surface. The value for $K^{\downarrow}$ is determined on the basis of standard astronomical equations (e.g. Iqbal, 1983), which lead to an instantaneous value of 1180 W m^{-2} incident to the top of the atmosphere at the centre of the watershed during Landsat overpass at 0945 hours. From Equation (1) a value for the two-way transmittance of $\tau''_{sw} = 0.35$ was obtained, which implies that the single-way transmittance is $\tau_{sw} = 0.59$. Hence, a portion of $1180 \times 0.59 = 696$ W m^{-2},

after atmospheric absorption, scatter and transfer will reach the land surface. A small, relatively flat area of 19 km × 25 km was studied, hence the effect of topography on radiation balance was not considered. The apparent emissivity of the atmosphere, $\varepsilon' = 0.91$, is obtained from the empirical relationship between ε' and T_a (Brutsaert, 1975). Incoming long-wave radiation is estimated by using air temperature and the apparent emissivity of the atmosphere, yielding a value of $\varepsilon'\sigma T_a^4 = L \downarrow = 407$ W m^{-2}. The screen-height air temperature during satellite overpass was $T_a = 24.8\,^\circ$C, being tentatively estimated from the surface temperature of Lake Naivasha ($T_0 = 24.8\,^\circ$C, unit 2 see Table II) assuming that $T_a \approx T_0$ above water. A similar condition for wet surface evaporation was observed by Prihodko and Goward (1997), who concluded that the surface temperature of an infinitely thick vegetation canopy is close to ambient air temperature. The outgoing long-wave radiation is derived from T_0 and ε_0 and varies for each hydrological unit.

The soil heat flux is classically expressed as

$$G_0 = \lambda_s \frac{\partial T_s}{\partial z} \qquad (\text{W m}^{-2}) \tag{9}$$

where $\partial T_s/\partial z$ (K m^{-1}) is the vertical gradient of temperature beneath the land surface and λ_s (W m^{-1} K^{-1}) is the apparent thermal conductivity. The value for G_0 cannot be determined from satellite spectral measurements. However, previous studies have shown that the G_0/R_n fraction can be estimated from NDVI (Daughtry *et al.*, 1990), T_0 (Menenti, 1984) or a combination of NDVI, T_0 and r_0 (Bastiaanssen and Roebeling, 1993). Daughtry *et al.*, (1990) obtained an absolute relative error of 13% between measured G_0 and estimated G_0 using the NDVI relationship. They observe that this is better than estimating G_0 simply as 10 or 20% of R_n, in which case absolute relative errors of 58 and 25%, respectively, occurred. The following expression, for the relationship between G_0 and R_n, validated for the HAPEX experiments in Spain and Niger (Bastiaanssen *et al.*, 1998a) was used

$$\frac{G_0}{R_n} = \frac{T_0^c}{r_0}(0.0032\,r_{0,\text{avg}} + 0.0062\,r_{0,\text{avg}}^2)(1 - 0.978\,\text{NDVI}^4) \qquad (-) \tag{10}$$

where T_0^c ($^\circ$C) is the instantaneous radiometric surface temperature expressed in degrees centigrade and $r_{0,\text{avg}}$ (−) is the average value of r_0 during daylight hours when heat is stored in the topsoil. For Landsat overpass in the mid-morning, r_0^{avg} can be estimated as $1.1r_0$ (Menenti *et al.*, 1989). The G_0/R_n relationship is not valid for water bodies. The value for G_0 for water therefore was calculated as 1% of R_n (Ashfaque, 1999).

Table III. Estimation of instantaneous radiation balance and net available energy ($R_n - G_0$)

Hydrological unit	K↓ (W m^{-2})	K↑ (W m^{-2})	L↓ (W m^{-2})	L↑ (W m^{-2})	R_n (W m^{-2})	ε_0 (−)	G_0 (W m^{-2})	$R_n - G_0$ (W m^{-2})
1	696	132	407	487	484	0.966	79	405
2	696	42	407	448	614	1.000	6	608
3	696	84	407	453	566	0.989	55	511
4	696	139	407	507	457	0.952	87	370
5	696	153	407	508	442	0.951	87	355
6	696	97	407	460	546	0.984	62	484
7	696	146	407	504	453	0.955	85	368
8	696	146	407	495	462	0.960	82	380
9	696	84	407	446	573	0.992	50	523
10	696	139	407	493	471	0.957	83	388
11	696	174	407	487	442	0.962	80	362
12	696	125	407	498	480	0.952	85	395
13	696	132	407	500	471	0.958	84	387
14	696	174	407	503	426	0.962	82	344
15	696	104	407	463	536	0.990	57	479

Table III shows the resulting R_n and G_0 values for the 15 hydrological units discerned. Unit 2 (open water) seems to have 608 W m^{-2} available energy ($R_n - G_0$) for sensible and latent heat fluxes, whereas unit 5, with 355 W m^{-2} absorbs significantly less energy owing to high reflected (K $\uparrow$= 153 W m^{-2}) and emitted radiation (L $\uparrow$= 508 W m^{-2}). These distinct spatial variations in $R_n - G_0$ will affect the SVAT parameters, surface energy balance and related hydrological processes.

*Partitioning of available energy into sensible and latent heat fluxes (*H *and* LE*)*

The sensible heat flux, H, is classically expressed as

$$H = \frac{\rho_a c_p}{r_{ah}} \delta T_a (\text{W m}^{-2}) \tag{11}$$

where ρ_a (kg m^{-3}) is the moist air density, c_p (J kg^{-1} K^{-1}) is the air specific heat at constant pressure, r_{ah} (s m^{-1}) is the aerodynamic resistance to heat transport and δT_a is the temperature difference between layer z_{down} and z_{up}. Figure 2 depicts the logarithmic temperature profile between a particular land surface type and the lower part of the atmospheric boundary layer. The sensible heat flux H of Equation (11) applies to the region between the lower (z_{down}) and upper (z_{up}) integration limits for the eddy diffusivity for heat transport, K_h

$$r_{ah} = \int_{z_{down}}^{z_{up}} \frac{1}{K_h} dz = \left[\frac{1}{ku*} \ln \left(\frac{z_{up}}{z_{down}} \right) - \psi_h \right] \qquad (\text{s m}^{-1}) \tag{12}$$

where u_* (m s^{-1}) is the friction velocity, k (–) is the von Karman's constant and ψ_h (–) is the stability correction of the temperature profile due to buoyancy (Brutsaert, 1982). Most often, the surface roughness for heat transport, z_{0h}, is taken as the lower integration limit in order to comply with the aerodynamic surface temperature, T_{z0h}. The major obstacle in practically using thermal infrared images for the estimation of sensible heat flux from radiometric surface temperatures T_0, is that $T_0 \neq T_{z0h}$ (Carlson *et al*., 1995). Figure 2 shows that the quantification of z_{down} modifies r_{ah}, δT_a and, following Equation (11), also H. Most thermal infrared studies are based on the hypothesis that $T_0 = T_{z0h}$ and z_{0h} is adjusted to match H (Kalma and Jupp, 1990; Lhomme *et al*., 1994). This can be done only if *in situ* measurements of H are available, which is not a straightforward situation. Although this solution gives satisfactory results for specific land cover classes for which z_{0h} can be calibrated, it does not permit applications of the calibrated z_{0h} values to other hydrological units with varying vegetation heights and biophysical conditions. Hence, an alternative solution has been worked out in order to apply Equations (11) and (12) in composite terrain. Bastiaanssen *et al*., (1998b) suggested to basically assume $T_{z0h} \neq T_0$ and take an arbitrary value of z_{down}. The temperature difference δT_a between z_{up} and z_{down} then can be established from r_{ah} and H without involvement of T_0 or T_a

$$\delta T_a = \frac{H r_{ah}}{\rho_a c_p} \qquad (\text{K}) \tag{13}$$

Equation (13) is more a matching of H by calibrating δT_a rather than by adjusting z_{0h}. This at the same time evades the necessity to have accurate and instantaneous T_a data from all over the watershed. It also eliminates problems induced by improper quantification of T_0 from remote sensing data using Equation 3. Figure 2 shows that δT_a can be calculated theoretically for any height z_{down}, however, a small value of z_{down} ($z_{down} \approx z_{0h}$) is preferred in order to comply better with the theory of thermodynamics. As *in situ* H fluxes for the Navaisha catchment were not available, H is estimated from the spatial variation of energy partitioning in the watershed. The solution of the sensible heat flux can be made by approximating water bodies to have a negligible sensible heat flux ($H \approx 0$; $R_n \approx G_0 + LE$). Experimental evidence that $H \approx 0$ W m^{-2} for water bodies was obtained by, for example, by de Bruin and Keijman (1979) for a 460 km^2 inland lake of 3 m depth and for Lake Naivasha by Ashfaque (1999). In contrast, extremely dry areas can be approximated to have a zero latent heat flux ($LE \approx 0$ and $H \approx R_n - G_0$). The $T_0(r_0)$ relationship (see Figure 6) is used to

correctly identify the wettest and driest units. The wettest areas have lowest T_0 and r_0, whereas the driest have highest r_0 and high T_0. Units 2 and 14 were identified as the wettest and driest units. The arguments described above can be used to estimate the energy balance of unit 2 as $R_n = 614$ W m^{-2}, $G_0 = 6$ W m^{-2}, $H = 0$ and $LE = 608$ W m^{-2} and $\delta T_a = 0$ K. Unit 14 is characterized by a surface energy balance of $R_n = 426$ W m^{-2}, $G_0 = 82$ W m^{-2}, $H = 344$ W m^{-2} and $LE = 0$ W m^{-2}. These two extremes in sensible heat flux are used to solve δT_a in Equation (13) if r_{ah} is known. This means that thermal infrared data are not used for estimating the thermal gradient.

Two turbulent structure parameters are essential for the computation of r_{ah}; friction velocity, u_*, and the Monin–Obukhov length, L. Menenti *et al.*, (1989) published first indications that r_{ah} can be obtained from the slope between remotely sensed r_0 and T_0. Bastiaanssen *et al.*, (1998b) describe an interative procedure to determine u_* and L, together with an estimate of z_{0h}, from the negative slope between T_0 and r_0. Following Moran and Jackson (1991), the surface roughness for momentum transport, z_{0m}, can be estimated from NDVI. In this study estimates of z_{0m} were made on the basis of experimental findings of Niger (Taylor *et al.*, 1997). The values of z_{0h} were taken a factor 10 lower (kB$^{-1} = 2\cdot3$), which provided the opportunity to estimate z_{0h} for each hydrological unit (see Table IV). The results of the interative procedure indicate an area-effective friction velocity, u_*^{eff}, of $0\cdot341$ m s^{-1}. This value was converted into area-effective wind speed at 100 m height by considering an area effective roughness length z_{0m}^{eff} and u_*^{eff} and using the flux–profile relationship for momentum transfer (Brutsaert, 1982). This gave a value of $u_{100} = 3\cdot9$ m s^{-1}. Local u_* values thereafter could be derived using z_{0h} and stability conditions ψ_h for every hydrological unit.

The near-surface vertical air temperature difference can be solved for unit 14 as $\delta T_a = 12\cdot1$ K after having determined $r_{ah} = 40\cdot2$ s m^{-1} and $H = 344$ W m^{-2}. Note that δT_a is obtained from Equation (14) and not deduced from $T_0 - T_a$. It is further known that low δT_a values coincide with low thermal emission ($T_0 = 24\cdot8$ °C) and that a high value of δT_a coincides with high thermal emission ($T_0 = 36\cdot7$ °C). A function between radiometric surface temperature T_0 and δT_a therefore was established. Experimental work in China (HEIFE: Wang *et al.*, 1995), USA(FIFE: Franks and Beven, 1997), Niger(HAPEX: (Troufleau *et al.*, 1997) and Egypt (Bastiaanssen *et al.*, 1998b) has indicated that the radiometric surface temperature is a linear function of δT_a. This relationship is the same for both land and water surfaces and applies to the space domain only and not to time. The relationship therefore is valid only for the time of satellite image acquisition and for a given region with a specific solar radiation and wind speed. For this study, δT_a has been computed for each hydrological unit using the self-calibration of units 2 ($T_0 = 24\cdot8$ and $\delta T_a = 0$ °C) and 14 ($T_0 = 36\cdot7$ and $\delta T_a = 12\cdot1$ °C)

$$\delta T_a = 1\cdot02\ T_0 - 25\cdot3 \qquad \text{(K)} \tag{14}$$

where T_0 is expressed in degrees centigrade. The iterative procedure for u_*, L, ψ_h, r_{ah} and H was applied to each hydrological unit separately, leading to the r_{ah} and H values presented in Table IV.
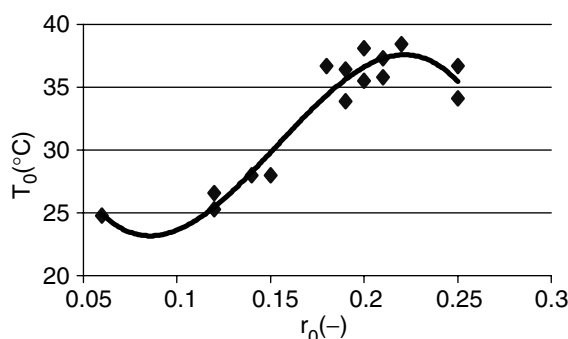

Figure 6. Relationship between surface temperature (T_0) and surface albedo (r_0)

Table IV. Estimation of instantaneous SVAT parameters and heat fluxes

Hydrological unit	z_{0h} (m)	u_* (m s^{-1})	L (m)	ψ_h (−)	δT_a (K)	r_{ah} (s m^{-1})	r_s (s m^{-1})	H (W m^{-2})	LE (W m^{-2})	Λ (−)
1	0·0055	0·36	−14·8	1·1	9·3	38·4	518	274	131	0·32
2	0·0031	0·27	∞	0·0	0·0	65·8	0	0	608	1·00
3	0·0500	0·63	−176·7	0·2	1·8	17·0	91	122	389	0·76
4	0·0024	0·31	−8·3	1·5	13·6	48·2	1840	319	51	0·14
5	0·0021	0·31	−7·9	1·5	13·9	49·4	2646	318	36	0·10
6	0·0276	0·52	−73	0·4	3·3	22·5	125	164	320	0·66
7	0·0028	0·32	−9·2	1·4	12·8	46·1	1637	314	54	0·15
8	0·0036	0·33	−11·2	1·3	11·0	43·4	848	288	91	0·24
9	0·0705	0·72	−784·5	0·0	0·5	14·2	64	40	482	0·92
10	0·0030	0·32	−10·8	1·3	10·9	46·1	631	268	120	0·31
11	0·0043	0·34	−13·5	1·2	9·5	42·0	652	256	106	0·29
12	0·0024	0·31	−9·2	1·4	12·1	49·2	714	280	115	0·29
13	0·0033	0·33	−10·3	1·4	11·8	44·2	985	304	84	0·22
14	0·0043	0·35	−10·8	1·3	12·1	40·2	∞	343	0	0·00
15	0·0546	0·68	−108·7	0·3	3·3	15·2	184	243	237	0·49

The transport equation for latent heat flux is given generally by

$$LE = \frac{\rho_a c_p}{\gamma(r_{av} + r_s)}\{e_{sat}(T_0) - e_{act}\} \qquad (\text{W m}^{-2}) \qquad (15)$$

where e_{sat} (mbar) is the saturated vapour pressure at surface temperature T_0 (inside stomata or soil cavity or at water−air interface for open water bodies), e_{act} (mbar) is the actual vapour pressure at screen height, γ (mbar K^{-1}) is the psychrometric constant, r_{av} (s m^{-1}) is the aerodynamic resistance to water vapour transport and r_s (s m^{-1}) is the bulk surface resistance to evaporation. The surface resistance, r_s, controls LE and hence the partitioning between H and LE. Unfortunately, r_s is difficult to quantify and varies, in addition to soil moisture, with solar radiation, vapour pressure deficit and air temperature (Jarvis, 1976; Stewart, 1988). As r_s is difficult to model, it is easier to express LE as a residual of the surface energy balance residual than to calculate it according to Equation (15)

$$LE = R_n - G_0 - H \qquad (\text{W m}^{-2}) \qquad (16)$$

From Table IV it can be seen that unit 9 (forest) consumes more water ($LE = 482$ W m^{-2}) than unit 3 ($LE = 389$ W m^{-2}) owing to the difference in the available energy $R_n - G_0$. Unit 15 evaporates 50% less than open water evaporation from Lake Navaisha ($LE = 237$ W m^{-2}). Unit 5 indicates a strongly reduced evaporation ($LE = 36$ W m^{-2}). To verify the physical consistency of the generally accepted micrometeorological equation (Equation 16), the surface resistance was obtained by inversion of Equation (15) after having determined LE from Equation (16) and assuming that $r_{ah} = r_{av}$. The saturated vapour pressure was computed as

$$e_{sat}(T_0) = 6\cdot11 \exp\left(\frac{17\cdot27 T_0}{T_0 + 237\cdot3}\right) \qquad (\text{mbar}) \qquad (17)$$

The actual vapour pressure was set at $e_{act} = 10$ mbar and obtained from unit 2, taking $LE = 554$ W m^{-2}, $r_{av} = 65\cdot5$ s m^{-1}, $e_{sat} = 31\cdot3$ mbar and $r_s = 0$ s m^{-1}. The lowest surface resistance next to open water with $r_s = 0$ s m^{-1}, is unit 9 with $r_s = 64$ s m^{-1}, followed by unit 3 with $r_s = 91$ s m^{-1}(see Table IV). Resistances of this magnitude reveal that forest and irrigated crops are transpiring at potential level. The food and agricultural organization (FAO) has defined $r_s = 70$ s m^{-1} as the resistance for an unstressed grass field (Allen et al., 1994), which is in agreement with the values obtained. Dolman (1993) gave values for tropical forests

in the range of minimally $r_s = 50$ s m^{-1}. Taylor *et al.*, (1997) gave a minimum resistance for dense bush land of 80 s m^{-1}. This shows that the estimations of the heat fluxes are in agreement with the expectations.

The evaporative fraction, Λ, was calculated from LE, R_n and G_0

$$\Lambda = \frac{LE}{R_n - G_0} \qquad (-) \tag{18}$$

The evaporative fraction is a fairly constant indicator of the energy partitioning during daylight hours and can be used to temporally integrate the energy balance from instantaneous values to 24-h values. Studies by Sugita and Brutsaert (1990) and Crago (1996), among others, have extensively indicated that the fraction as defined in Equation (18) is temporally constant. Because of forcing unit 2 with $H = 0$ and unit 14 with $LE = 0$, the evaporative fraction varies between 0 and 1 (see Table IV). The 24-h actual evaporation is computed according to the net radiation on 24 h, R_{n24}, and Λ using

$$ET_{24} = \Lambda R_{n24} \qquad (\text{mm day}^{-1}) \tag{19}$$

R_{n24} is obtained as follows

$$Rn_{24} = (1 - r_0^{\text{avg}})K \downarrow_{24} + L *_{24} \qquad (\text{W m}^{-2}) \tag{20}$$

where $K \downarrow_{24}$ is the solar radiation integrated over 24 h calculated from solar hour angle and the Sun zenith angle at the time of over pass of the satellite (Iqbal, 1983), and $L*_{24}$ is the net long-wave radiation for 24 h and is calculated by semi-empirical function presented by Allen *et al.*, (1998). The results of Equation (19) are presented in Table V and displayed in Figure 7. The estimated lake evaporation on 21 January is 6·5 mm day^{-1}. Unit 9 (forest) has 5·5 mm day^{-1}, whereas units 3 (cropland), 4 and 7 (grasslands/rangelands) have an evaporation of 4·5 mm day^{-1} and 0·7 mm day^{-1}, respectively. The reference evaporation for grass computed with the Penman–Monteith equation, as precisely described in Allen *et al.*, (1994) gives 5·8 mm day^{-1}. This reference evaporation of unstressed grass compares with the actual evaporation of unit 9 (5·5 mm day^{-1}) and is more than unit 3 (4·5 mm day^{-1}).

Table V. Estimation of 24-hour time integrated estimated evaporation

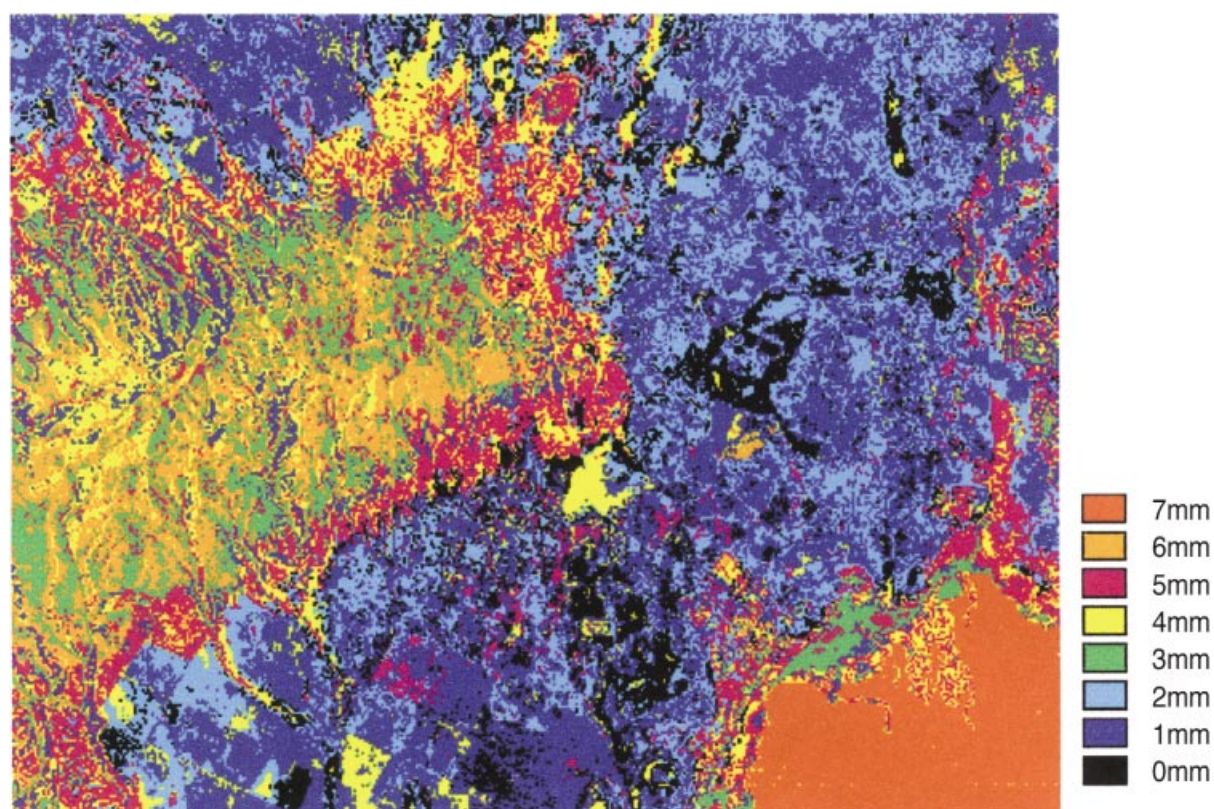| Hydrological unit	Λ (−)	R_{n24} (W m^{-2})	ET_{24} (mm day^{-1})
1	0·32	149	1·7
2	1·00	184	6·5
3	0·76	168	4·5
4	0·14	146	0·7
5	0·10	141	0·5
6	0·66	163	3·8
7	0·15	144	0·7
8	0·24	144	1·2
9	0·92	168	5·5
10	0·31	147	1·6
11	0·29	133	1·4
12	0·29	152	1·6
13	0·22	149	1·2
14	0·00	133	0·0
15	0·49	160	2·8

Figure 7. Spatial patterns of actual evaporation in the Lake Navaisha watershed on 21 January 1995

VALIDATION

The validation of surface parameters and fluxes determined by remote sensing is a difficult task. In the ideal situation fluxes should be measured simultaneously in all the hydrological units at the time of overpass of the satellite. This usually is not possible, however owing to limitations of the available technical and financial resources to obtain field data from a heterogeneous landscape. Furthermore the fluxes obtained from ground measurements are limited in areal extent and representative of a relatively small area as compared with those obtained from remote sensing algorithms. Hence validation of regional scale evaporation is not straightforward.

Field data obtained from two field campaigns conducted in October 1998 and January 1999 were used for validation. Data from a meteorological station also were available for the period 1961–1968. During October 1998, air temperature, air humidity and wind speed were measured at two levels. Incoming and outgoing radiation were measured separately. In January 1999, air temperature and air humidity at three levels(0·1 m, 2 m and 3 m), rainfall and incoming solar radiation were measured at 20 min intervals by an automatic weather station placed in a dry grassland area 5 km west of Lake Naivasha. The equipment used were a Kipp and Zonen pyranometer with a sensitivity of 9·07 μV watt^{-1}m^{-2} and measuring range of 0·305–2·8 μm, temperature and humidity sensors with an accuracy of ±0·01 °C and 1% relative humidity respectively, and a psychrometer with an accuracy of 0·2 °C.

Table VI shows air temperature at 2 m height, short-wave atmospheric transmittance and evaporative fraction at 0940 hours local time from 18 to 31 January 1999, determined from the field measurements. Daily evaporation from the grassland site and from open water (Lake Naivasha) were also computed from the field data. The Bowen ratio energy balance method was used to calculate evaporation from the two

Table VI. Comparison of measured and estimated evaporation

Date	Solar radiation at top of atmosphere (W m^{-2}) (0940 hours)	Solar radiation at surface (W m^{-2}) (0940 hours)	Atmo-spheric transmission (−) (0940 hours)	Air tempe-rature (2 m) °C (0940 hours)	Evapora-tive fraction (−) (0940 hours)	Evapo-ration (unit7) (mm day^{-1})	Evapo-ration water (unit2) (mm day^{-1})
18-1-99	1095	671	0·61	23·5	0·47	0·7	5·0
19-1-99	1097	670	0·61	22·6	0·34	1·5	4·8
20-1-99	1098	656	0·60	23·2	0·27	0·7	5·8
21-1-99	1099	639	0·58	23·6	0·26	0·5	5·8
22-1-99	1100	642	0·58	23·7	0·20	1·6	4·9
23-1-99	1101	658	0·60	22·6	0·25	0·4	6·0
24-1-99	1102	668	0·61	24·3	0·16	0·5	6·5
25-1-99	1104	675	0·61	22·9	0·15	0·5	6·7
26-1-99	1105	680	0·61	23·6	0·09	0·5	6·4
27-1-99	1106	671	0·61	23·0	0·11	0·0	6·8
28-1-99	1107	668	0·60	22·8	0·12	0·0	6·7
29-1-99	1109	661	0·60	23·6	0·11	0·0	5·9
30-1-99	1110	653	0·59	23·6	0·41	0·7	5·5
31-1-99	1111	690	0·62	24·7	0·29	1·0	6·7
Average			0·60	23·4	0·23	0·6	6·0
Estimated from remote sensing			0·59	24·8	0·21	0·7	6·5

sites. Table VI also shows the results from remote sensing for comparison. The automatic weather station in the grassland site was located in unit 7. The average field measured Λ and evaporation were 0·23 and 0·61 mm day^{-1} respectively. This compares well with the values of 0·21 and 0·70 mm day^{-1} obtained from remote sensing. For open water evaporation a value of 6·0 mm day^{-1} was obtained from field measurement as opposed to 6·5 mm day^{-1} from remote sensing. The two sites selected for validation represent the two extremes of wetness conditions. It therefore is expected that the results from the other hydrological units are also in the correct range. At 0940 hours, when Landsat passes over, there is little variation of τ during the 14 days of observations. The highest value was 0·62 and the lowest was 0·58, with an average of 0·60. It is evident that the value of 0·59 obtained from the simple expression used to estimate τ (Equation 1) is valid. The air temperature is between 22·6 and 24·7 °C, with an average of 23·4 °C. A value of 24·8 °C was used in this remote sensing study, being determined from the average surface temperature of Lake Naivasha assuming zero heat flux, and this also seems reasonable.

Table VII shows daily solar radiation, daily atmospheric transmissivity and evaporation (open water) extracted for the month of January of records (1961–1968) from Kedong meteorological station situated in the study area. The mean value of lake evaporation from the long term data is 6·4 mm day^{-1}. This reveals that

Table VII. Long-term data for the month of January (1961–1968)

	Minimum(mean)	Mean	Maximum(mean)
Daily solar rad(w/m^2)	244	266	282
Daily Tranmissivity(−)	0·58	0·64	0·67
Evaporation (open–water) (mm day^{-1})	5·8	6·4	6·8

lake evaporation depicted in Table V is reliable. Figure 8(A–C) shows graphs of surface and air temperature, albedo and surface fluxes against time measured over Lake Naivasha on 8 October 1998. Figure 8A supports the assumptions that the air temperature over moist surfaces, such as water, is approximately equal to the surface temperature. The average difference is $1\,^\circ$C, with the minimum and maximum differences being $0\,^\circ$C and $2\cdot1\,^\circ$C respectively. Figure 8B indicates that albedo is about $0\cdot06$ between 1000 and 1100 hours. Albedo varies during the day, however, with lowest ($0\cdot03$) observed between 1300 and 1400 hours. The surface fluxes in Figure 8C indicate that R_n is very close and almost equal to LE, showing that Λ is approximately equal to 1 (Ashfaque, 1999). Both H and G_0 over water are close to zero. This agrees with the estimations presented in Table IV.

The validation of results from similar studies in Egypt, Spain, China and Niger (Kustas *et al.*, 1994; Bastiaanssen *et al.*, 1998a; Wang et al., 1998), which had extensive data from large-scale field experiments, indicates that reliable estimates of evaporation can be obtained from remotely sensed data. Root mean square error (RMSE) of between $0\cdot05$ and $0\cdot14$ are reported for Λ, and differences between ground-based measurements and estimated evaporation from remote sensing are between 5% and 20%. Sensitivity analysis indicated that 25% change in the parameters caused less than 20% change in the fluxes and Λ. $K\downarrow$, r_0 and T_0 were the most sensitive parameters in estimating the fluxes.

AGGREGATION OF SVAT PARAMETER AND FLUXES

Aggregation rules of SVAT parameters have been used to calculate the area-representative SVAT parameters for the Navaisha watershed. Aggregated parameters usually are applied as input in land surface parameterization
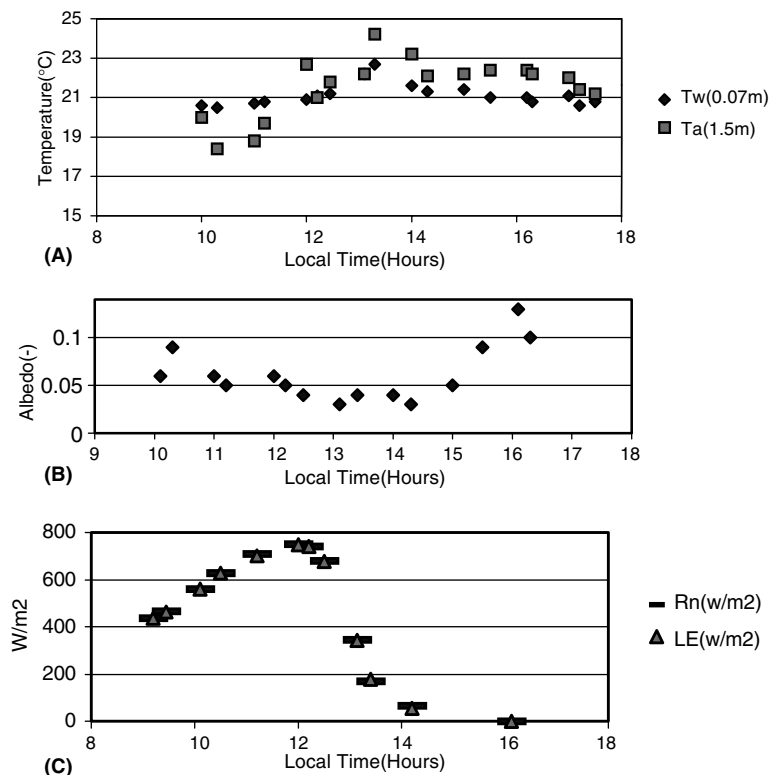

Figure 8. (A) Temperature profiles measured over Lake Naivasha. (B) Albedo measurements over Lake Naivasha. (C) Surface fluxes measured over Lake Naivasha

schemes for the simulation of large-scale energy balances and exchange processes between land and atmosphere (e.g. Noilhan *et al.*, 1997). In this study, however, area-representative parameters will be used to analyse the effect of spatial variations of the SVAT parameters on evaporation. A comparison will be made between fluxes of each hydrological unit calculated from local SVAT parameters *vis-a-vis* fluxes obtained using area-aggregated SVAT parameters.

Many different aggregation rules have been published in recent years (e.g. McNaughton *et al.*, 1994; Shuttleworth, 1998). In the current study, r_0, ε_0, z_{0m}, u_*, ψ_h and δT_a SVAT parameters have been areally aggregated. The regionally representative surface albedo is calculated as the weighted mean of the values of the individual hydrological units because variations in cloud cover did not exist on the cloud-free image of 21 January and the size of the area is sufficiently small and relatively flat to allow extraterrestrial radiation to be constant

$$r_0^{\text{eff}} = \sum a_i r_{0i} \qquad (-) \tag{21}$$

where, r_0^{eff} is the area-effective albedo, a_i and r_{0i} are the fractional area coverage and surface albedo respectively for a particular class i. Data on fractional area a_i are presented in Table II. The results show $r_0^{\text{eff}} = 0.177$. The aggregated surface thermal infrared emissivity was determined from a weighting scheme, using both the fractional area a_i as well as the emitted black body radiation

$$\varepsilon_0^{\text{eff}} = \frac{\sum a_i \varepsilon_{0i} \sigma T_{0i}^4}{\sum a_i \sigma T_{0i}^4} \qquad (-) \tag{22}$$

Following Wang *et al.* (1998), Equation (22) assigns more weight to the areas having a higher thermal radiation. The results show that $\varepsilon_0^{\text{eff}} = 0.968$. Regional surface temperature is determined by using area effective emissivity obtained from Equation (22) and upwelling radiation

$$T_0^{\text{eff}} = \left(\frac{\sum a_i \varepsilon_{0i} \sigma T_{0i}^4}{\varepsilon_0^{\text{eff}} \sigma} \right)^{0.25} \qquad (\text{K}) \tag{23}$$

The results show that $T_0^{\text{eff}} = 33.2\,^\circ\text{C}$. The surface roughness length for heat transport was aggregated according to the procedure of Mason (1988), being developed for the aggregation of the surface roughness length for momentum transport

$$\frac{1}{[\ln(z_B/z_{\text{oh}}^{\text{eff}})]^2} = \sum \frac{a_i}{[\ln(z_B/z_{0hi})]^2} \qquad (-) \tag{24}$$

The above expression is based on the idea that the factor $[\ln(z_B/z_{\text{oh}})]^2$ is linearly related to friction velocity and that the area-representative sensible heat flux appears at some height above the land surface where all fluxes from individual surface elements are blended out as a result of turbulent mixing. This blending height, z_B, was taken as 100 m elevation. The results show $z_{0h}^{\text{eff}} = 0.0041$ m. The friction velocity u_* was aggregated according to the momentum flux weighted for fractional area a_i

$$u_*^{\text{eff}} = \left[\frac{\sum a_i \rho_a (u_{*i})^2}{\rho_a} \right]^{0.25} \qquad (\text{N m}^{-2}) \tag{25}$$

The result shows $u_*^{\text{eff}} = 0.341$ m s^{-1} which agrees with u_*^{eff} obtained from the interative procedure. This implies that the disaggregation/aggregation procedure for u_* is consistent. The stability correction factor ψ_h is

an integral part of the aerodynamic resistance r_{ah} (see Equation 13). Values for ψ_h were aggregated by using the standard expression of the Monin–Obukhov length using u_*^{eff}, T_0^{eff} and H^{eff}

$$L^{eff} = -\frac{\rho_a c_p (u_*^{eff})^3 T_0^{eff}}{kgH^{eff}} \qquad (m) \qquad (26)$$

where g (m s^{-2}) is the acceleration due to gravity and H^{eff} is the weighted average of all H_i fluxes ($\sum a_i H_i$). The results show that $\psi_h = 1\cdot11$. The area-effective value for $\delta T_a^{eff} = 8\cdot5$ K was obtained from a weighted average

$$\delta T_a^{eff} = \sum a_i \delta T_{a-i} \qquad (K) \qquad (27)$$

PARAMETER VARIABILITY AND IMPACT ON SURFACE FLUXES

Watershed average surface fluxes

A parameter variability study is performed to provide an indication of the importance of schematizing the spatial variability of SVAT parameters. First, the effect on total watershed H and LE fluxes will be discussed, followed by the effect on spatially distributed H and LE fluxes.

The Lake Naivasha watershed surface energy balance is calculated from the aggregated SVAT parameters using Equation (8) for R_n^{eff}, Equation (10) for G_0^{eff} (taking NDVI^{eff} = 0·28) and Equation (11) for H^{eff}. The results are presented in Table VIII. It appears that H^{eff} has a 2·3% deviation from $\sum a_i H_i$ and LE^{eff} a 4·0% deviation from $\sum a_i LE_i$. These differences are within the error of estimation of the fluxes. It therefore can be concluded that the aggregation rules yield satisfactory results to assess area-effective surface fluxes. Hence total watershed evaporation can be obtained satisfactorily from area-aggregated SVAT parameters and there is no need to solve the evaporation from subcatchments explicitly. It is, however, required to describe accurately the spatial variation of SVAT parameters and sound aggregation rules should be applied rather than arithmetic mean values of SVAT parameters. As parameter values in Table IV differ considerably from the values of the aggregated SVAT parameters, it may be concluded that the incorporation of local measured SVAT parameters for calculating watershed fluxes can lead to erroneous results.

Watershed distributed surface fluxes

Two different treatments of the parameter domains on watershed-distributed surface fluxes are tested: locally estimated SVAT parameters of Table IV versus spatially constant SVAT parameters. The watershed-aggregated values of SVAT parameters were used as spatially constant over the whole watershed. The fluxes of each unit are calculated by taking alternatively each of the parameters, shown in Tables IX and X, as equal to the watershed-aggregated parameter. The deviation of these fluxes from the fluxes calculated using distributed parameters (Table IV) is represented as a percentage of the fractional difference

$$\frac{Y_i(x_1 \cdots x_n) - Y_i(x^{eff}, x_1 \cdots x_{n-1})}{Y_i(x_1 \cdots x_n)} \times 100 \qquad (\%) \qquad (28)$$

Table VIII. Total watershed energy balance as a weighted average of energy balances from the 15 hydrological units and from area-aggregated SVAT parameters

Flux (W m^{-2})	Weighted average of hydrological units	Area-aggregated SVAT parameters
Net radiation	497	496
Soil heat flux	77	79
Sensible heat flux	221	226
Latent heat flux	199	191

Table IX. Fractional difference of the latent heat flux variations of the hydrological units resulting from variations of SVAT parameters

Hydro-logical unit	δT_a (K)	z_{oh} (m)	u_* (m s^{-1})	ψ_h (−)	r_0 (−)	ε_0 (−)	Root-mean-square percentage fractional difference
1	+19·8	+6·3	+18·1	+7·8	+5·4	+0·1	11·9
2	−26·2	0·0	0·0	0·0	−15·7	+1·4	12·5
3	−112·9	+11·1	+15·1	−6·2	−10·7	−0·7	47·0
4	−239·2	−77·3	−36·4	+55·6	+27·4	−2·3	106·7
5	+345·9	−122·2	−66·0	+80·4	+77·0	−3·6	158·8
6	−81·1	+14·0	+18·9	−6·2	−8·9	−3·6	34·8
7	+197·7	−52·6	−16·3	+46·6	+38·4	−0·3	87·3
8	+74·7	−13·8	+3·8	+19·6	+22·9	−1·5	33·4
9	−130·3	+3·3	+4·5	−2·2	−8·8	−0·6	53·4
10	+51·6	−16·6	−5·6	+14·5	+11·3	−0·9	23·5
11	+27·5	−3·3	+8·5	+10·9	+45·6	−0·6	22·5
12	+74·9	−29·6	−16·6	+19·1	0	−1·5	34·5
13	+105·5	−21·6	0·0	+25·7	+8·4	−0·9	43·3
14	+114794	−5160·4	+20366·8	+25417·7	+81060	−0·5	58929·2
15	−161·7	+37·9	+52·6	−17·7	+9·0	+221·8	115·4
Root-mean-square percentage fractional difference	147·7	43·8	26·8	31·5	28·8	1·7	

where Y_i represents the sensible or latent heat flux of unit number i and x represents the SVAT parameters. Tables IX and X summarize how fluxes of the hydrological units vary when spatially constant SVAT parameters are considered instead of local distributed values. Generally, the units can be divided into three groups on the basis of their sensitivity. The wet units 2 and 9 are relatively less sensitive for *LE* but most sensitive to *H*. The wet units have large values for *LE*, for example 554 W m^{-2} for unit 2. Absolute LE deviations owing to changes in the SVAT parameters yield small fractional differences. The dry units 13 and 14 are very sensitive to *LE* but less sensitive for *H* estimations. The third group (e.g. units 1 and 8) are insensitive in the estimations of both *H* and *LE* because local parameter values are similar to the spatially constant values selected, i.e. the aggregated values. The aggregated regional values of the parameters are $u_*^{eff} = 0·341$ m s^{-1}, $z_{0h}^{eff} = 0·0041$ m, $\psi_h^{eff} = 1·11$ and $\delta T_a^{eff} = 8·5$ K, and the values at unit 1 are $u_* = 0·36$ m s^{-1}, $z_{0h} = 0·0056$ m, $\psi_h = 1·14$ and $\delta T_a = 9·3$ K.

The estimation of evaporation from individual hydrological units is most sensitive to δT_a (mean root square fractional difference of 147·7%). The surface roughness length for heat transport is the second most sensitive parameter in the estimation of *LE* (root mean square fractional difference of 43·8%). Unit 14 is the most sensitive to z_{0h} in the estimation of *LE*, with a percentage difference of −5160%, whereas unit 2 is the least sensitive, with a value of 0·0%. It is important to note that use of u_*^{eff}, ψ_h^{eff} and r_0^{eff} also considerably affects the calculation of local evaporation, with root mean square fractional differences varying between 26·8% and 31·5%. Only usage of ε_0^{eff} seems to be acceptable. More caution is thus required for the calculation of distributed fluxes in watersheds using areal constant SVAT parameters. This issue has so far not been properly addressed in the scientific community of remote sensing based surface energy balances.

Table X. Fractional difference of the latent heat flux of the hydrological units resulting from variations of SVAT parameters

Hydro-logical unit	δT_a (K)	z_{oh} (m)	u_* (m s^{-1})	ψ_h (−)	r_0 (−)	ε_0 (−)	Root-mean-square percentage fractional difference
1	−9·4	−3·0	−8·6	−3·7	0·0	−0·2	5·5
2	−210100	+5·7	+20·1	+14·2	0·0	−5255	85799·8
3	+358·5	−35·1	−48·0	+19·6	0·0	+9·6	148·6
4	−38·1	+12·3	+5·8	−8·8	0·0	−1·3	16·9
5	−39·4	+13·9	+7·5	−9·2	0·0	−1·5	17·7
6	+157·7	−27·2	−36·7	+12·0	0·0	+4·1	67·2
7	−34·1	+9·1	+2·8	−8·0	0·0	−1·6	14·8
8	−23·7	+4·4	−1·2	−6·2	0·0	−0·8	10·2
9	+1560·1	−39·3	−54·4	+25·9	0·0	+32·6	637·7
10	−23·0	+7·4	+2·5	−6·5	0·0	−1·1	10·3
11	−11·4	+1·3	−3·5	−4·5	0·0	−0·6	5·2
12	−30·8	+12·1	+6·8	−7·8	0·0	−1·5	14·2
13	−29·0	+5·9	0·0	−7·1	0·0	−0·9	12·4
14	−30·8	+1·4	+5·5	−6·8	0·0	−0·5	13·1
15	+157·7	−36·9	+51·3	+17·3	0·0	+5·6	69·7
Root-mean-square percentage fractional difference	234·2	19·3	25·7	12·1	0·0	9·3	9·3

CONCLUSIONS

A new method has been presented to quickly delineate a heterogeneous watershed into hydrological units, without having access to ground data, by using remotely sensed data. The difference in hydrology is based on only the remote sensing determined surface temperature, NDVI and surface albedo. This remote sensing method does not describe land use or land cover and therefore can be applied even without identifying training areas. A watershed delineation is necessary to describe variations in soil–vegetation–atmosphere–transfer parameters and the related fluxes. The schematization into a limited number of hydrological units allows the computation of the energy balance in a spread sheet. The spatial variation of SVAT parameters is difficult to measure in the field. Therefore literature has been cited and used to estimate the areal patterns of SVAT parameters from spectral Landsat TM data. Field data obtained in two field campaigns held in October 1998 and January 1999 and long-term meteorological data were used to verify the results. The actual evaporation of water and dry grassland agreed with those calculated from data collected in January 1999. The evaporation of water obtained was also within range of those calculated from long-term data (1961–1968) for the month of January. The resulting surface resistance varied for wet surfaces between 0 and 91 s m^{-1}, which is very likely and agrees with published figures. The method proposed can be applied, under cloud-free conditions, at any watershed, river basin or irrigation scheme having heterogeneity in land surface.

The results of the parameter variability analysis and the effect on fluxes show that δT_a is the most sensitive parameter, followed in importance by z_{0h}, u_*, ψ_h and r_0. This implies that air temperature variability needs to be described properly. The total evaporation from a catchment can be estimated accurately from area-aggregated SVAT parameters, provided that these area-representative values are obtained through the aggregation rules given in Equations (21) to (27) and are based on distributed SVAT parameters over the entire watershed. The

consequence of this finding is that the spatial variations of SVAT parameters have to be described under all circumstances, even for calculating area-averaged watershed surface fluxes. Existing energy balance models using remotely sensed input data for distributed watershed evaporation therefore should be re-examined for their suitability of parameterizing spatial variability in SVAT parameters. Most published algorithms in the literature appear not to be suitable for calculating watershed distributed evaporation (e.g. algorithms in classes 1, 2, 3 and 4 in Table I).

REFERENCES

Allen RG, Smith M, Pereira LS, Perrier A. 1994. An update for the calculation of reference evapotranspiration. *ICID (International Committee on Irrigation and Drainage) Bulletin* **43**(2): 35–92.

Allen RG, Preira LS, Raes D, Smith M. 1998. *Crop Evapotranspiration: Guidelines for Computing Crop Water Requirements*. FAO Irrigation and Drainage Paper 56, Food and Agriculture Organization: Rome.

Ase LE, Sernbo K, Syren P. 1986. *Studies of Lake Navaisha, Kenya, and its Drainage Area*. STOU-NG 63, Institute of National Geography, Stockholm University: ISSN 0346-7406, 79 pp.

Ashfaque A. 1999. *Estimating lake evaporation using meteorological data and remote sensing*. MSc thesis, International Institute of Aerospace Survey and Earth Sciences—ITC: Enschede, The Netherlands; 93 pp.

Baret F, Guyot G. 1991. Potentials and limits of vegetation indices for LAI and APAR assessment. *Remote Sensing of the Environment* **35**: 161–173.

Bastiaanssen WGM, Roebeling RA. 1993. Analysis of land surface exchange processes in two agricultural regions in Spain using Thematic Mapper Simulator data. In *Exchange Processes at the Land Surface for a Range of Space and Time Scales*, Bolle, Feddes, Kalma (eds). IAHS Publications (International Association of Hydrological Sciences: Wellingford; Vol. 212, 407–416.

Bastiaanssen WGM, Menenti M, Dolman AJ, Feddes RA, Pelgrum H. 1996. Remote sensing parameterization of meso-scale land surface evaporation. In *Radiation and Water in Climate System: Remote Measurements*, Rascheke E (ed.). NATO ASI series 1, Vol. 45, Springer-verlag: Berlin; 401–429.

Bastiaanssen WGM, Pelgrum H, Wang J, Ma Y, Moreno JF, Roerirink GJ, van der Wal T. 1998a. A remote sensing surface energy balance algorithm for land (SEBAL), part 2: validation. *Journal of Hydrology* **212–213**: 213–229.

Bastiaanssen WGM, Menenti M, Feddes RA, Holtslag AAM. 1998b. A remote sensing surface energy balance algorithm for land (SEBAL), part 1: formulation. *Journal of Hydrology* **212–213**: 198–212.

Blyth EM. 1994. *The effect of small scale heterogeneity on surface heat and moisture fluxes*. PhD thesis, University of Reading, Department of Meteorology: 152 pp.

Brutsaert W. 1975. On a derivable formula for long-wave radiation from clear skies. *Water Resources Research* **11**: 742–744.

Brutsaert W. 1982. *Evaporation into the Atmosphere, Theory, History and Applications*. Reidel: Dordrecht; 299 pp.

Brutsaert W, Hsu AY, Schmugge TJ. 1993. Parametrization of surface heat fluxes above forest with satellite thermal and boundary layer soundings. *Journal of Applied Meteorology* **32**: 909–917.

Carlson TN, Buffum MJ. 1989. On estimating total daily evapotranspiration from remote surface temperature measurements. *Remote Sensing of the Environment* **29**: 197–207.

Carlson TN, Taconet O, Vidal A, Gillies RR, Olioso A, Humes K. 1995. An overview of the workshop on thermal remote sensing held at La Londe les Maures, France, September 20–24, 1993. *Agriculture and Forest Meteorology* **77**: 141–151.

Chen D, Engman ET, Brutsaert W. 1997. Spatial distribution and pattern persistence of surface soil moisture and temperature over prairie from remote sensing. *Remote Sensing of the Environment* **61**: 347–360.

Choudhury BJ. 1991. Multispectral satellite data in the context of land surface heat balance. *Review of Geophysics* **29**: 217–236.

Choudhury BJ, Ahmed NU, Idso SB, Reginato RJ, Daughtry CST. 1994. Relations between evaporation coefficients and vegetation indices studied by model simulations. *Remote Sensing of the Environment* **50**: 1–17.

Crago RD. 1996. Conservation and variability of the evaporative fraction during the daytime. *Journal of Hydrology* **180**: 173–194.

Daughtry CST, Kustas WP, Moran MS, Pinter PJ, Jackson RD, Brown PW, Nichols WD, Gay LW. 1990. Spectral estimates of net radiation and soil heat flux. *Remote Sensing of the Environment* **39**: 141–152.

De Bruin HAR, Keijman JQ. 1979. The Priestley–Taylor evaporation model applied to a large, shallow lake in the Netherlands. *Journal of Applied Meteorology* **18**: 893–903.

Diak G, Wipple MS. 1993. Improvements to models and methods for evaluating the land-surface energy balance and effective roughness using radiosonde reports and satellite measured skin temperature data. *Agriculture and Forest Meteorology* **65**: 21–45.

Dolman AJ. 1993. A multiple-source land surface energy balance model for use in general circulation models. *Agriculture and Forest Meteorology* **65**: 21–45.

Donia NS. 1998. *Integration of GIS and computer modelling to study the water quality of Lake Navaisha, Central Rift Valley, Kenya*. MSc thesis, International Institute of Aerospace Survey and Earth Sciences—ITC, Enschede, The Netherlands: 116 pp.

Franks SW, Beven KJ. 1997. Estimation of evapotranspiration at the landscape scale: a fuzzy disaggregation approach. *Water Resources Research* **33**: 2929–2938.

Hamududu BH. 1998. *Erosion assessment of large basins using remote sensing and GIS: a case study of lake Naivasha basin Kenya* MSc thesis, International Institute of Aerospace Survey and Earth Sciences—ITC, Enschede, The Netherlands: 123 pp.

Heckbert PS. 1994. *Graphic gems IV*, AP Professional: Boston.

Iqbal M. 1983. *An introduction to solar radiation*. Academic Press: Toronto.

Jackson RD. 1984. Total reflected solar radiation calculated from multi-band sensor data. *Agriculture and Forest Meteorology* **33**: 163–175.

Jackson RD, Reginato RJ, Idso SB. 1977. Wheat canopy temperature: a practical tool for evaluating water requirements. *Water Resources Research* **13**: 651–665.

Jarvis PG. 1976. The interpretation of the variations in leaf water potential and stomatal conductance found in canopies in the field. *Philosophical Transactions of the Royal Society of London, Series B* **273**: 593–610.

Kalma JD, Jupp DLB. 1990. Estimating evaporation from pasture using infrared thermography: evaluation of a one-layer resistance model. *Agriculture and Forest Meteorology* **51**: 223–246.

Koepke P, Kriebel KT, Dietrich B. 1985. The effect of surface reflection and of atmospheric parameters on the shortwave radiation budget. *Advances in Space Research* **5**: 351–354.

Kustas WP, Norman JM. 1996. Use of remote sensing for evapotranspiration monitoring over land surfaces. *Hydrological Sciences Journal* **41**(4): 495–516.

Kustas WP, Moran MS, Humes KS, Stannard DI, Pinter PJ, Hipps LE, Swiatek E, Goodrich DC. 1994. Surface energy balance at local and regional scales using optical remote sensing from aircraft platform and atmospheric data collected over semiarid rangelands. *Water Resources Research* **30**: 1241–1259.

Lhomme JP, Monteny B, Amadou M. 1994. Estimating sensible heat flux from radiometric temperature over sparse millet. *Agriculture and Forest Meteorology* **68**: 77–91.

Markham BL, Barker JL. 1987. Thematic Mapper bandpass solar exoatmospherical irradiances. *International Journal of Remote Sensing* **8**(3): 517–523.

Mason P. 1988. The formulation of areally averaged roughness lengths. *Quarterly Journal of Royal Meteorological Society* **114**: 399–420.

McNaughton KG. 1994. Effective stomatal and boundary layer resistances of heterogeneous surfaces. *Plant, Cell and Environment* **17**: 1061–1068.

Menenti M. 1984. *Physical aspect and determination of evaporation from deserts*. ICW Report 4, DLO-Winand Staring Centre, PhD thesis, Wageningen Agricultural University, The Netherlands.

Menenti M, Bastiaanssen WGM, Van Eick D, Abd el Karim MH. 1989. Linear relationships between surface reflectance and temperature and their application to map actual evaporation of groundwater. *Advances in Space Research* **9**(1): 165–176.

Menenti M, Choudhury BJ. 1994. Synergetic use of thermal infrared and other spectral measurements for land surface studies. *Proceedings, Workshop on Thermal Remote Sensing*, La Londe, September 1993; 167–176.

Moran MS, Jackson RD. 1991. Assessing the spatial distribution of evapotranspiration using remotely sensed inputs. *Journal of Environmental Quality* **20**: 7225–737.

Moran MS, Maas SJ, Pinter PJ. 1995. Combining remote sensing and modeling for estimating surface evaporation and biomass production. *Remote Sensing Review* **12**: 335–353.

Nemani RR, Running SW. 1989. Estimation of regional surface resistance to evapotranspiration from NDVI and thermal-IR AVHRR data. *Journal of Applied Meteorology* **28**: 276–284.

Noilhan J, Lacarrere P, Dolman AJ, Blyth EM. 1997. Defining area-average parameters in meteorological models for land surfaces with mesoscale heterogeneity. *Journal of Hydrology* **190**: 302–316.

Pelgrum H, Bastiaanssen WGM. 1997. The non-linearity between surface fluxes and remotely observable land surface characteristics and its consequences for pixel size selection. *Thirteenth Conference on Hydrology*: 2–7 February, Longbeach, California, American Meteorological Society, **P8. 3**; 342–344.

Pinty B, Ramond D. 1987. A method for the estimate of broadband directional surface albedo from a geostationary satellite. *Journal of Climate and Applied Meteorology* **26**: 1709–1722.

Prihodko L, Goward SN. 1997. Estimation of air temperature from remotely sensed surface observations. *Remote Sensing of the Environment* **60**: 335–346.

Rosema A. 1990. Comparison of meteosat-based rainfall and evapotranspiration mapping sahel region. *International Journal of Remote Sensing* **11**(12): 2299–2309.

Schmugge T, Hook SJ, Coll C. 1998. Recovering surface temperature and emissivity from thermal infrared multispectral data. *Remote Sensing Environment* **65**: 121–131.

Seguin B, Itier B. 1983. Using midday surface temperature to estimate daily evaporation from satellite thermal IR data. *International Journal of Remote Sensing* **4**: 371–383.

Shuttleworth WJ, Yang ZL, Arain MA. 1998. Aggregation rules for surface parameters in global models. *Hydrology and Earth System Sciences* **2**: 217–226.

Stewart JB. 1988. Modelling surface conductance of pine forest. *Agriculture and Forest Meteorology* **43**: 339–353.

Sugita M, Brutsaert W. 1990. Regional surface fluxes from remotely sensed skin temperature and lower boundary layer measurements. *Water Resources Research* **26**: 2937–2944.

Tanre D, Deroo C, Duhaut P, Herman M, Morcette JJ, Perbos J, Deschamps PY. 1990. Description of a computer code to simulate the satellite signal in the solar spectrum: the 5S code. *International Journal of Remote Sensing* **11**: 659–668.

Taylor CM, Harding RJ, Thorpe AJ, Bessemoulin P. 1997. A mesoscale simulation of land surface heterogeneity from HAPEX—Sahel. *Journal of Hydrology* **188–189**: 1040–1066.

Troufleau D, Lhomme JP, Monteny B, Vidal A. 1997. Sensible heat flux and radiometric surface temperature over sparse Sahelian vegetation. I, An experimental analysis of the kB^{-1} parameter. *Journal of Hydrology* **188–189**: 815–838.

Tucker CJ. 1979. Red and photographic infrared linear combination for monitoring vegetation. *Remote Sensing of the Environment* **8**: 127–150.

Valor E, Caselles V. 1996. Mapping land surface emissivity from NDVI: application to European, African and South American areas. *Remote Sensing of the Environment* **57**: 167–184.

Van de Griend AA, Owe M. 1993. On the relationship between thermal emissivity and the normalized difference vegetation index for natural surfaces. *International Journal of Remote Sensing* **14**(6): 1119–1131.

Wang J, Ma Y, Menenti M, Bastiaanssen WGM, Mitsuta Y. 1995. The scaling up of processes in the heterogeneous landscape of HEIFE with the aid of satellite remote sensing. *Journal of the Meteorological Society of Japan* **73**(6): 1235–1244.

Wang J, Bastiaanssen WGM, Ma Y, Pelgrum H. 1998. Aggregation of land surface parameters in the oasis–desert systems of northwest China. *Hydrological Processes* **12**: 2133–2147.

Zhong Q, Li YH. 1988. Satellite observation of surface albedo over the Qinghai–Xizang plateau region. *Advances in Atmospheric Sciences* **5**: 57–65.